Frontiers in Heat and Mass Transfer (FHMT), 20, 15 (2023)
DOI: 10.5098/hmt.20.15

Global Digital Central
ISSN: 2151-8629

Frontiers in Heat and Mass Transfer

Available at www.ThermalFluidsCentral.org

ASYMMETRIC PHENOMENON OF FLICKERING FLAME UNDER DIFFERENT CO-FLOW VELOCITIES

Wenhua Liu[a,b], Mo Yang[c,a,*], Yuwen Zhang[b], Guiliang Liu[a], Liang Ling[a], Xuchen Ying[a,*]

[a] *School of Power and Energy Engineering, University of Shanghai for Science and Technology, Shanghai, 200093, China*
[b] *Department of Mechanical and Aerospace Engineering, University of Missouri, Columbia, MO 65211, USA*
[c] *Shanghai Jianqiao University, Shanghai, 201306, China*

ABSTRACT

In this study, numerical investigations are performed on a partially premixed flame of methane and air in two- and three-dimensional models. Nonlinear method is adopted to illustrate the asymmetric phenomenon that affects the flame stability under various co-flow velocities. According to the results, the mathematical relationship between the flame flickering frequency Stanton number and the dimensionless velocity Froude number has been summarized as $St=0.7Fr^{-0.46}$. The bifurcation phenomena under different Reynold numbers are found to have significant influence on the system stability. Two critical bifurcation points, which is when Re=300 and Re=1200, are determined as the onset of breaking the flame symmetry and the onset of chaotic state, respectively. The research on flame flicker characteristics provides valuable reference for engineering applications in stable combustion and other related fields.

Keywords: *Flickering flame, Asymmetric phenomenon, Nonlinear characteristics, Stable combustion*

1. INTRODUCTION

Combustion systems are the most typical thermal flows system associated with a rapid chemical reaction, and they also belong to complex nonlinear systems with turbulent flow and chemical kinetics (e.g., the exponential dependence of reaction rate on temperature). The instability of the flame will affect the combustion efficiency of the combustion equipment, generate pollutants, and even cause the combustion equipment to flame out in extreme cases (Massa and Freund, 2017). Hence, the periodic and chaotic motions in flame dynamics that can be observed as a result of flame instabilities are of fundamental importance to present combustion science (Sayed-Kassem et al., 2021; Xu et al., 2022; Bae et al., 2022; Manikantachari et al., 2011).

Flickering flame is a manifestation of unstable flame combustion, and the buoyant force driven by natural convection makes a significant impact on generating flame instabilities (Krikunova et al., 2022; Zhu et al., 2022). As for diffusion flames, the entire flow field predominantly consists of high-temperature combustion products behind the flame front and low-temperature surrounding air. When high-temperature combustion products are accelerated by an upward buoyant force interact with the low-temperature surrounding air, the interface between the flows becomes unstable owing to the hydrodynamic shear layer instability associated with the Kelvin-Helmholtz instability mechanism, resulting in the appearance of vortexes at the interface. As the vortexes develop and move downstream, they interact with the flame front to distort the flame shape and induce large oscillations in amplitude owing to the Rayleigh-Taylor instability mechanism. The periodic oscillation of the flame front generated by these processes is referred to as the flickering flame. Its dynamic study is significant for understanding the transition from a laminar flame to a turbulent flame. Ahmad et al. (2022) investigated the diffusion of flickering flame by experimental method, and the results prove that flickering instability could be suppressed by only controlling the air surrounding the flame. Researchers have conducted investigations of flickering flame under various combustion cases experimentally. Yoshihara et al. (2013) conducted an experimental investigation on flame characteristics under different gravity levels and captured the flickering flame with a high-speed camera. Fujisawa et al. (2014) experimentally investigated an axisymmetric premixed methane/air flame under the influence of co-flow using the image analysis and the flame reaction technique, and the results showed different co-flow velocities. Their following research (Fujisawa and Okuda, 2018) focused on the flickering flame with different air co-flow and equivalence ratios and found that the flickering motion weakens at high equivalence ratios. Whereas researchers often ignore the nonlinearity of the complex system and numerical analysis of the flame combustion process from the perspective of nonlinearity with its bifurcation phenomenon (Oyewola, et al., 2021; Mohammadpour, et al., 2022). Therefore, when the flame flicker phenomenon occurs in the experiment, researchers consider it the result of certain disturbances. Besides, the two-dimensional and three-dimensional models have been used in some investigations (Yamamoto et al., 2004; Hariharan and Wichiman, 2014), however, there are few reports about the differences in numerical results of flickering flame between different models.

A better understanding of the nonlinearity, e.g., asymmetric phenomenon, in a system is critical to both preventing nonlinear influence (when system stability is needed) and elevating engineering nonlinearity (when system performance is desired) (Yang, 2018; Sciamanna and Shore, 2015; Ying et al., 2022). Li et al. (2019,2021) numerically investigated the heat and mass transfer in a horizontal cavity. The novelty focused on the bifurcation and asymmetrical phenomenon which can be guided for other numerical simulations in related fields. Wang et al. (2013) studied the diffusion flame frequency behavior with the change of high-temperature gas flow structure through experiments adopting the nonlinear theory as guidance. Recently, Araya et al. (2022) found that the oscillatory state appeared from the stationary state through

* *Corresponding authors. Email: moyang0626@gmail.com (Mo Yang), yingxuchen@hotmail.com (Xuchen Ying)*

Global Digital Central
ISSN: 2151-8629

the subcritical Andronov-Hopf bifurcation both in simulation and experiment and visualized the vortex structure. Their results showed that both the excitation frequency and amplitude play a dominant role in the flame oscillation frequency. Singh et al. (2022) investigated the effect of the obliquity of the co-axial swirling flame jet and noticed asymmetric recirculation lobes have been used for the co-axial swirling flame. The study of the nonlinear bifurcation phenomenon of premixed flame is helpful for the exploration of the flame instability mechanism and the control of stable combustion in engineering. The investigation of the dynamic behavior of the flame instability observed in this study by time series analysis in combination with a surrogate data method is essential for obtaining a more comprehensive understanding and interpretation of complex nonlinear phenomena in flame dynamics, which has not been explored in detail in the field of combustion science.

This study aims to investigate the flickering mechanism and nonlinear characteristics of a partially premixed flame of methane/air through nonlinear dynamic analysis. The numerical experiments are conducted on the validated two-dimensional and three-dimensional models, respectively. A fitted curve of the St number and the Fr number has been carried out, which is close to the experimental results in literature. The bifurcation phenomena under different Reynolds numbers are elaborated, and three key bifurcation points which affect the system stability are found. The results obtained in this paper will provide essential guidance for improving the flame stability in combustion system.

2. PHYSICAL MODEL AND BASIC EQUATIONS

2.1 Physical Model

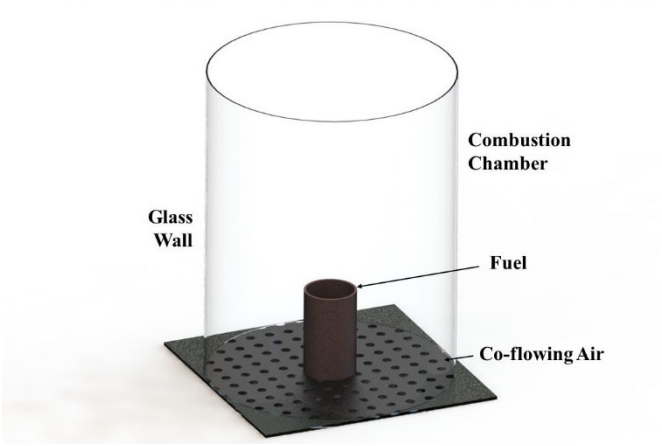

Fig. 1 3D Physical Model

The physical model in this paper is a co-axial jet premixed burner, in which air and methane are premixed first in the mixing chamber (Fig.1). The inlet of the combustion chamber is composed of two co-axial cylindrical tubes. The fuel is emitted from the inner tube area, and the co-flow air is pumped into the annular area between the inner and outer tubes. The mixture of fuel and oxidizer reacts in the combustion chamber surrounded by glass wall.

The methane and air in the tube are mixed with certain equivalent ratio. The temperature of the mixture is set 298 K. The numerical simulation default pressure is 1 atmosphere, and the gravitational acceleration is 9.8 m/s^2. The commercial software FLUENT was used as the solver to calculate the governing equations.

2.2 Mathematical Model

The governing equations for the fluid flow and heat transfer of the combustion process can be written as:

$$\nabla \cdot (\rho v) = 0 \tag{1}$$

$$\frac{\partial(\rho v)}{\partial t} + \nabla \cdot (\rho v v - \mu \nabla v) = -\nabla p + \nabla(\mu \nabla v), \tag{2}$$

$$\frac{\partial(\rho T)}{\partial t} + \nabla \cdot \left(\rho v T - \frac{\lambda}{c_p}\nabla T\right) = S_h, \tag{3}$$

$$\frac{\partial(\rho Y_i)}{\partial t} + \nabla \cdot (\rho v Y_i) = -\nabla J_i + R_i + S_i, \tag{4}$$

where, S_h is the heat of chemical reaction or some other defined volume source term, including the radiant heat loss from a flame; R_i is the net formation rate of component *i* due to chemical reactions; S_i is the net production rate of component *i* due to discrete term and other custom source terms, J_i is the diffusion density of component *i*.

In this paper, a multi-component ideal gas mixture is considered, and the ideal gas state equation is written as,

$$\rho = \frac{p}{\bar{R}T}, \tag{5}$$

where, $\bar{R}$ is gas constant, which is defined as $\bar{R} = R/\bar{M}$.

The combustion model is a mathematical representation of the chemical reaction kinetic factors in the combustion process of reactive fuel. In this paper, a simplified two-step chemical reaction model of methane is adopted to simulate the chemical reaction kinetics of the methane combustion process, which is written as,

$$CH_4 + O_2 = CO + H_2O, \tag{6}$$

$$CO + 0.5\,O_2 = CO_2, \tag{7}$$

According to the Arrhenius law, the chemical reaction rate of the reaction equation $X_1 + X_2 = X_3$ can be expressed in terms of the reactant concentration as shown in the following equation, which is calculated by,

$$k = \frac{\partial(Y_{X_1})}{\partial t} = -AT^{\beta}\, exp(-\frac{E}{RT})\, Y_{X_1}, Y_{X_2}, \tag{8}$$

where, X_1 and X_2 are the concentrations of reactants X_1 and X_2; A is the pre-factor, β is the temperature index; E is the activation energy. Here, parameters were selected according to GRI-Mech 3.0 reaction mechanism. For reaction (6), $A = 5.012 \times 10^{11}$, $\beta = 0$, $E = 2 \times 10^8 J/(kg \cdot mol)$; and for reaction (7), $A = 2.239 \times 10^{11}$, $\beta = 0$, $E = 1.7 \times 10^8 J/(kg \cdot mol)$; in the reverse reaction, $A = 5 \times 10^8$, $\beta = 0$, $E = 1.7 \times 10^8 J/(kg \cdot mol)$.

3. MODEL VALIDATION AND NUMERICAL SIMULATION

3.1 Grid Independence Test

Meshing is one of the most critical steps in numerical simulation. The meshing quality directly affects the calculation's speed and precision. Therefore, based on the purpose of both satisfying the calculation accuracy and saving the computational cost, the numerical simulation research should select as few high-quality and accurate grids as possible. In this paper, three different grids are designed for the independence analysis. Since the research object of this paper is the combustion of methane-air coaxial jet flame, the combustion reaction mainly occurs near the central axis of the cylindrical calculation area, and the gradient changes of temperature, velocity, and other parameters in this area are drastic, so the three grids are encrypted in the central area.

This paper adopts a physical model with fuel inlet diameter *d* with 24 mm for comparison of grid independence analysis. Three kinds of grids are 0.85 million, 1.12 million, and 1.5 million, respectively. The calculation conditions are set according to the literature (Bennett et al., 2000); the specific situation is: the inner pipe (fuel inlet) is fed with a mixed gas with an equivalence ratio of φ is 1.2, and the fuel inlet velocity u_f is 0.22 m/s; the co-flowing air inlet is fed with an oxygen content of 0.232, and the co-flowing air inlet velocity u_c is 0.352 m/s, the velocity ratio of co-flowing air U_r ($U_r = u_c / u_f$) is 1.6, and the inlet gas temperature is 298 K; the gravity is along the Z-axis direction, the acceleration of gravity is 9.8 m/s^2, and the pressure is 1 atmosphere. The axial temperature distribution in the three-dimensional calculation domain

Global Digital Central
ISSN: 2151-8629

obtained by simulation is shown in Fig. 2. Figure 2 illustrates that the temperature distributions obtained using three distinct mesh densities exhibit remarkable similarity. Furthermore, Fig. 3 indicates that the distribution of final combustion products, calculated using varying mesh densities, is essentially uniform along the axis. This suggests that all three mesh densities meet the simulation requirements of this study. The results show that all three grids can meet the simulation requirements of this paper. Due to computational and time cost constraints, the model with 1.12 million grids was selected as the computational grid of the present research.

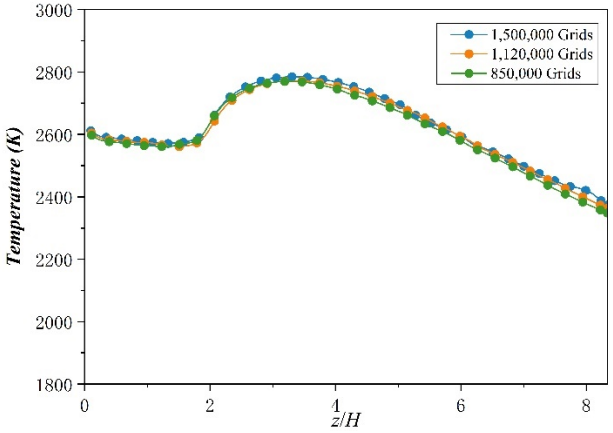

Fig. 2 Grid independence (Temperature distribution along the axis)

3.2 Model Validation

To further verify the calculation method's reliability, the comparison was made with different experimental results. Validation Case A is from Fujisawa's experiment (Fujisawa et al., 2014). As in **Table 1**, the specific working condition is: the diameter of the outer tube (co-flowing inlet) *D* is 95.2 mm, the diameter of the inner tube (fuel inlet) *d* is 11.4 mm, and the height of the combustion chamber *H* is 200 mm; the fuel inlet feeds the gas mixture with an equivalence ratio φ of 12.32, and the fuel inlet velocity u_f is 0.0928 m/s. Co-flowing air with an oxygen content of 0.232 is fed into the co-flowing air inlet, and the co-flowing air inlet velocity u_c is 0.1048 m/s. The velocity ratio of co-flowing air U_r is 1.13. The inlet fuel temperature is 298 K.

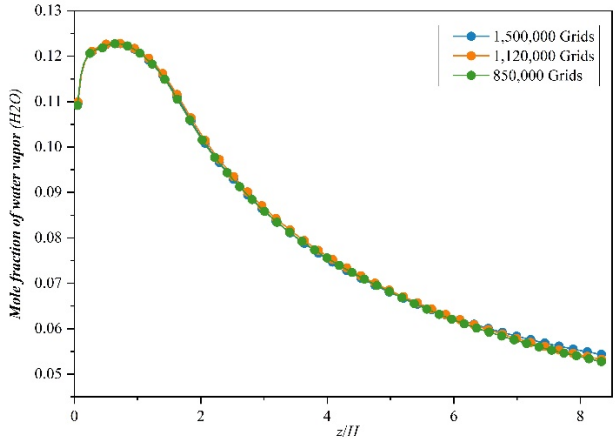

Fig. 3 Grid independence (The distribution of molar concentration of H2O along the axis)

To better verify the numerical method presented in this paper, three sets of different numerical simulations are set: a 2D axisymmetric model, a 3D model without radiation, and a 3D radiation model. The comparison between numerical results and experimental results is shown in Fig. 4, where H_T represents the height of the highest flame temperature along Z-axis. Compared with the 2D axisymmetric model, the calculation results obtained by the 3D model are closer to the experimental results. The calculation results considering the radiation model are more acceptable to the experimental results than those without the radiation model. The gap between the four curves at the maximum flame temperature is the largest. The triatomic gases (such as CO_2 and H_2O) generated by methane combustion in the air have a radiation effect on the combustion process. The magnitude of radiant heat loss directly affects the flame temperature and other parameters. The radiation model is indispensable in the calculation model adopted in the related numerical simulation. Considering the radiation effect, the three-dimensional model calculates that the maximum flame temperature on the axis is 2089K, and the relative error is 6.6% compared with the maximum experimental measured results of 1960K. The results show that the 3D model with radiation model can simulate the stable combustion of methane-air flame more accurately than the 2D axisymmetric model.

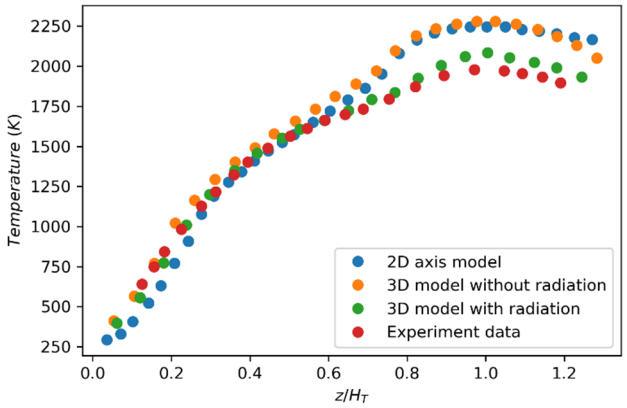

Fig. 3 Validation compared with experiment results

The calculated results are further verified with the experimental results of flame temperature distribution with *d* of 24 mm (Fujisawa et al., 2014). This verification case is noted as case B, and the specific conditions are: the diameter of the outer tube (co-flowing inlet) *D* is 154 mm, the diameter of the inner tube (fuel inlet) *d* is 24 mm, and the height of the combustion chamber *H* is 200 mm; the fuel inlet feeds the gas mixture at an equivalence ratio of 1.2, and the fuel inlet velocity u_f is 0.22 m/s. The co-flowing air inlet velocity u_c is 0.352 m/s. The velocity ratio of co-flowing air U_r is 1.6. The inlet fuel temperature is 298 K.

Table 1 Validation case condition

Name	*Case A*	*Case B*
D (mm)	95.2	154
d (mm)	11.4	24
H (mm)	200	200
φ	12.3	1.2
u_f (m/s)	0.0928	0.22
u_c (m/s)	0.1048	0.352
U_r (m/s)	1.13	1.6

Figure 5 shows the relevant results of flow field temperature obtained by simulation under validation case B. The flame surface of each result is relatively smooth and steady, indicating that the flame under validation case B is in the stable state. By comparing the flame image taken by the camera and the temperature distribution contour obtained by the tomographic reconstruction algorithm, it is found that the results obtained by the two-dimensional axisymmetric model and the 3D model are similar to the actual flame morphology in the literature. But the flame temperature of the 2D model is higher. Figure 5 reveals discernible disparities in the flame state between models of different

dimensions. This observation can be attributed to the complexity inherent in the flame combustion system. In complex systems, three-dimensional combustion systems are more prone to perturbations and consequently exhibit marked asymmetry. On the other hand, two-dimensional models tend to be more stable, thereby exhibiting less significant deviations. The transient calculation is adopted to simulate the combustion problem of unsteady methane flame in the following part, and the flicker characteristics are also investigated.

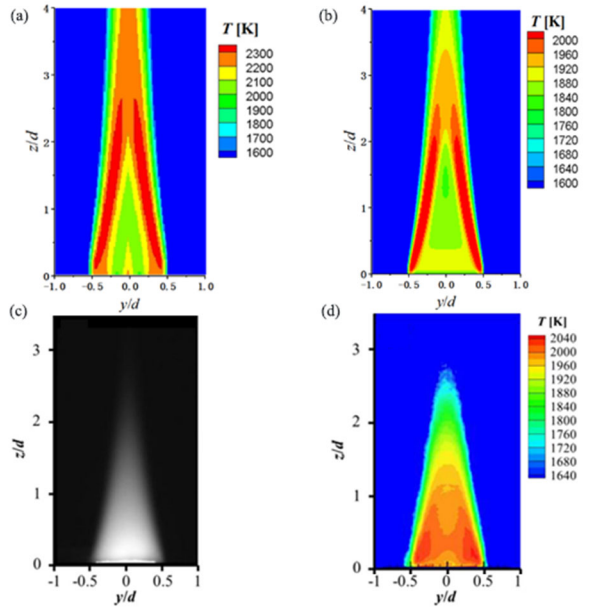

Fig. 4 Validation of balanced condition of flame (a) Temperature contour of the 2D-axisymmetric model (b) Temperature contour of the 3D model (c) Experiment shortcut (Fujisawa et al., 2014) (d) Tomographic reconstruction algorithm temperature contour (Fujisawa et al., 2014)

Flame combustion is a transient problem, the equation contains a time term and the calculated time step value at the same time. In the present study, the time step value of 10^{-5} was chosen for calculation purposes. The SIMPLE algorithm is used to solve the pressure and velocity coupling equation. For flame combustion with strong volume force flow, use PRESTO! perform pressure dispersion. The convection and diffusion terms are discretized by the QUICK and second-order upwind schemes, respectively. Whether the iteration convergences are judged according to the monitoring residual values: the residual values of the continuity equation and momentum equation are less than 10^{-5}; the residual values of the energy equation are less than 10^{-8}; the residual values of each component in the component transport equation are less than 0.001.

4. RESULTS AND DISCUSSIONS

4.1 Heat Transfer Characteristics of Flickering Flame

Figure 6 is the temperature distribution contour changes of 2D and 3D flame within 0.6s, respectively. The flame morphology presents a concave-convex structure over time, indicating that the flame is already flickering currently. The flame flow field is unstable in the absence of accompanying air, and a vortex structure is formed around the flame. The vortex structure continuously diffuses towards the Z-axis and enrolls the surrounding fluid due to the buoyancy force, resulting in a curvy structure on the flame surface.

The 2D model is a half domain model, as shown in Fig. 6 (a). The flame shape is deformed after being squeezed by the vortex and changes in the Z-axis direction with the vortex movement. In Fig. 6 (b), it is found that the flame temperature distribution obtained by three-dimensional simulation also produces deformation after being squeezed by vortexes. The difference is that the flame temperature distribution map not only shows stretching in the Z-axis direction but also shows the center deviation in the X-axis direction.

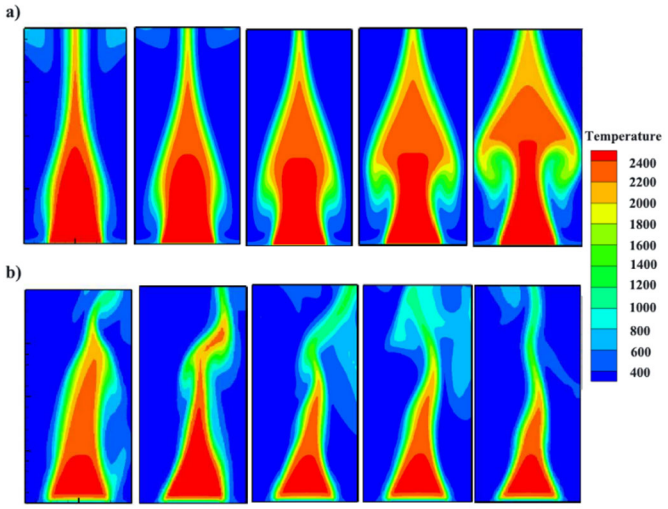

Fig. 5 Temperature contour in 0.6s (a) 2D model (b) 3D model

Table 2 shows the relative error between the flame scintillation frequency calculated under the 2D model and 3D model and the experimental data[11]. The relative error between the flame scintillation frequency calculated by the three-dimensional model and the experimental value is 4%. In contrast, the relative error is as high as 61% for the two-dimensional symmetric model, which means that for the nonlinear process of flame combustion, relying on the symmetry model cannot reflect the actual physical phenomenon changes and accurately predict the law of flame movement. It is more accurate to use a 3D model for the simulation of flame scintillation without the accompanying air velocity.

Table 2 Comparison of flame flicker frequency

Methods	*F(Hz)*	*Relative error*
2D simulation	5.289	61%
3D simulation	13	4%
Experimental data	12.5	-

4.2 Effect of Fuel Inlet Velocity

To further study the influence of fuel inlet velocity on flame stability, numerical investigations with different fuel inlet velocities are carried out in this paper. The setting details are shown in Table 3. The fuel inlet Reynolds number is a dimensionless parameter for differentiation study.

Table 3 Different fuel inlet conditions

u_f *(m/s)*	*Re*	U_r *(m/s)*
0.408	300	0.353
0.544	400	0.265
0.680	500	0.212
0.816	600	0.176
0.975	717	0.148
1.630	1200	0.088

Through the comparison of different test cases, it is found that there are three key points representing the state transition of the different flickering flames. Fig. 7 shows the typical temperature time series diagram under three different fuel inlet velocities. The monitoring point selected by the research is located 100mm from the Z-axis. The ratio of the peak temperature oscillation amplitude of the corresponding

Global Digital Central
ISSN: 2151-8629

monitoring point to the ambient temperature is 0.18%, 17.8%, and 10%, respectively. The numerical results show that the flame is in a stable combustion state when Re=300 and the flame is in an unstable combustion state when Re=500 and Re=1200. It is worth noting that in Fig. 6 (b), the amplitude of flame temperature under Re=500 is higher than that under Re=1200. This is because the height of the flame increases as the fuel flow increases, and the higher temperature region of the flame is at the top. The three temperature monitoring points are all located at the same height. Under the condition of Re=500, the monitoring points are close to the top of the flame, so the temperature amplitude of the monitoring points is significant.

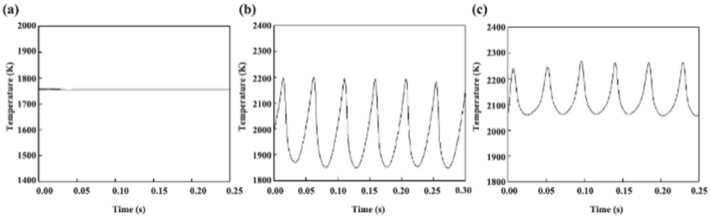

Fig. 6 Time series of temperature: (a) Re=300; (b) Re=500; (c) Re=1200

Figure 8 is the temperature distribution contour of flame burning instantaneously at a certain point. From the temperature time series graph in Fig. 7, it can be seen that the flame is in a stable state, and the flame shape does not change instantaneously. At this time, the flame surface has no curvy structure, indicating that the fuel velocity is smaller than that of the accompanying air, which can restrain the flame flicker state from around to ensure flame stability.

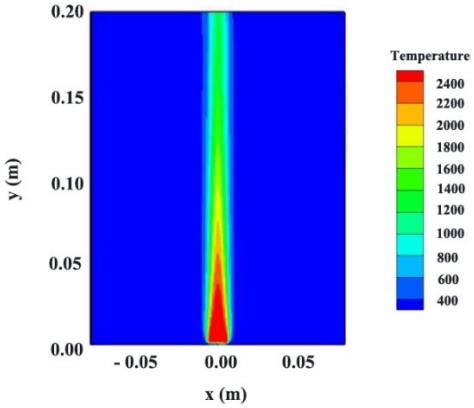

Fig. 7 Temperature contour of the flame

Figure 9 shows the contour of flame temperature distribution at the cross-section during the flicker period (0.0423s). By comparison with Figure 8, it is found that the flame shape is more flexuous because the energy released increases with the increment of fuel flow. With the increasing of fuel velocity, the temperature gradient near the flame surface rises further, and the flow field shows instability by forming a large-scale vortex structure. Vortices stretch the flame in the flow field from the X and Z directions, and the tilting degree enlarges with the Reynolds number. Moreover, the amplitude of the flame top increases obviously in the X-axis due to the vortex effect.

In addition to the qualitative analysis of the effect of fuel incidence velocity on flickering flame, the quantitative analysis between flickering flame and injection velocity is also provided by introducing the dimensionless parameter Fr, which is defined as,

$$Fr = \frac{{u_f}^2}{gd}, \tag{9}$$

where u_f is the fuel inlet velocity, g is the neutral acceleration, and d is the diameter of the burner.

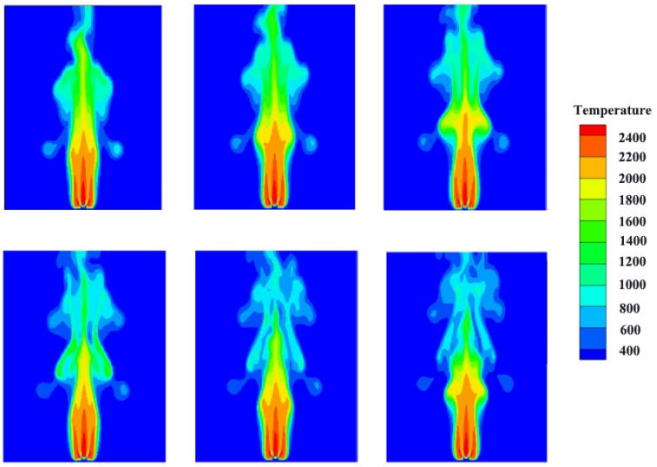

Fig. 8 Temperature contour distribution when Re is 1200

Figure 10 shows the fitting curve of the numerical calculation results with the calculation data. The correlation for the normalized variation St and Fr can be obtained as,

$$St = 0.7Fr^{-0.46}, \tag{10}$$

where the fitting standard deviation is 1.03%. From the experimental study of Fujisawa et al. (2014) and Fujisawa and Okuda (2018), the relation between the dimensionless flickering frequency and Fr is obtained, which is close to the research results in this paper, by which the calculated results are further verified.

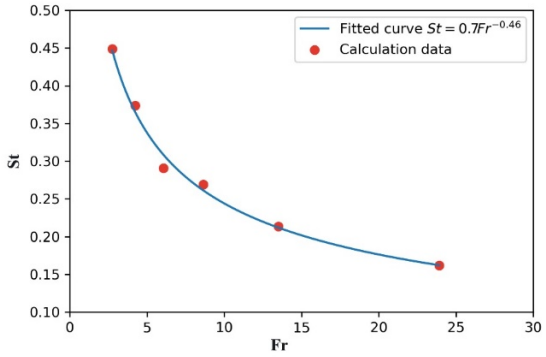

Fig. 9 Correlations of Stanton number and Froude number

4.3 Nonlinear Characteristic Analysis

Figure 11 shows the flame instantaneous temperature distribution contour as Re changes. When Re=300, the flame is in the stable combustion state, and the flame structure and temperature distribution are symmetrical along the Z-axis. When Re=500, the flame began to flicker, but the bottom remained stable. The temperature distribution contour showed a basically symmetrical structure with a slightly asymmetric deviation at the top of the flame. When Re=1200, the deviation degree of the top flame increases, showing an apparent asymmetric structure in the temperature distribution.

The numerical results show that even if the geometry and the boundary conditions of the burner are symmetric, the numerical results can still be asymmetric. With the increase of Re, the flame combustion process will change from stable to unstable flickering. The flame structure and temperature distribution will evolve from a symmetric structure to an asymmetric one. This means that the combustion system has multi-solution characteristic. There are both stable solutions and unstable oscillatory solutions reflecting as symmetric flame structure and asymmetric structure, respectively, which is the basic characteristic of a complex nonlinear system.

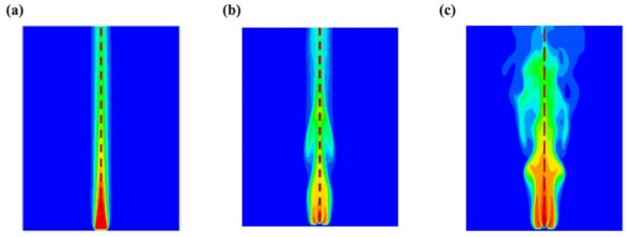

Fig. 10 Instantaneous temperature distribution contour: (a) Re=300; (b) Re=500; (c) Re=1200

In the experiments, Zhang et al. (2021) captured the transition of ethylene diffusion flame flickering from varicose flickering to sinuous flickering through high-speed photography. Therefore, the change of flickering flame types can be explained as when varicose flickering occurs, the flame is affected by the asymmetric disturbance of the annular vortex, and its temperature distribution exhibit a central asymmetric structure; when the sinuous flickering occurs, the flame oscillations appear at the top of the flame, the vortex deviates around the central axis of the flame, and the temperature contour exhibits an asymmetric structure.

Figure 12 shows the power spectrum under different Re numbers by performing Fast Fourier Transformation on the temperature at the monitoring point of the 3D model. When Re=300, there is no fundamental frequency or frequency multiplication in the power spectrum, indicating that the system is stable. When Re=500, the fundamental frequency and frequency multiplication appear in the power spectrum. The fundamental frequency is 22.38Hz, and the frequency multiplication is 41.56Hz, 63.94Hz, and 83.12 Hz, respectively. When Re=1200, the fundamental frequency also appears in the power spectrum. Under this condition, the fundamental frequency is 26.09Hz, and the frequency multiplication is 52.17Hz.

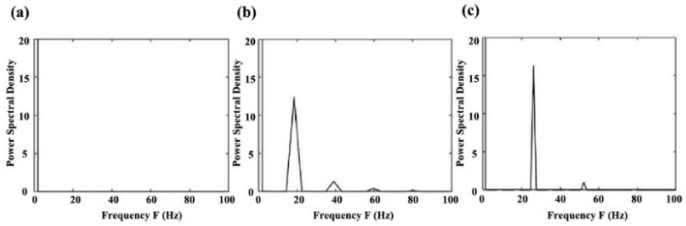

Fig. 11 Power spectrum: (a) Re=300; (b) Re=500; (c) Re=1200

Figure 13 is the phase portraits of velocity in three directions measured at the monitoring point with different Re numbers. The change in the flame state can be found more clearly in the velocity phase portrait. When Re=300, the phase space attractor is shown as a point. When Re=500, the system periodically oscillates, and the corresponding phase space trajectory is a period-doubling attractor, offering an "8"-shaped structure, and the surrounding orbits shrink to a torus. When Re=1200, the system is also in the period-doubling oscillation state, and the corresponding phase space attractor shrinks into the"8"-shaped torus.

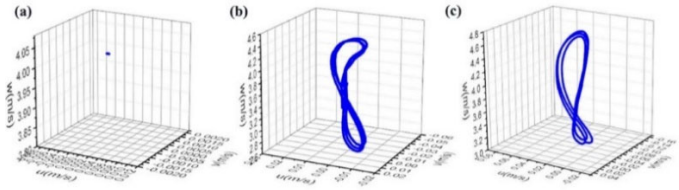

Fig. 12 Phase portraits of velocity: (a) Re=300; (b) Re=500; (c) Re=1200

The results above indicate that when the fuel velocity is increased, the combustion system enters a period-doubling oscillation state from a stable state, indicating that the system has a dynamic bifurcation phenomenon. The phase trajectory structure changes from a point to the "8" shaped structure, which is a nonlinear phenomenon unique to nonlinear systems. The fundamental frequency and the multiplication frequency appear in Fig.12, indicating that the system is bifurcated. It is predicted that as the fuel flow increases, the solution will continue to bifurcate, the power spectrum will change from discrete to continuous and finally enter a chaotic state.

In our forthcoming research, we plan to conduct numerical simulations to investigate the flame dynamics under various flow conditions, including small and large Reynolds numbers, and uniform turbulence. Our aim is to gain a deeper understanding of the flame behavior of coaxial jet premixed burners. Moreover, identifying the critical parameters that affect the chaotic bifurcation of these burners is of paramount importance.

5. CONCLUSIONS

In this paper, numerical simulation is used to study the effects of co-flow air velocity and fuel equivalent ratio on flame flicker frequency and its nonlinear characteristics. The numerical results agree well with the experimental results. Major conclusions obtained are as follows:

(1) The Reynolds number at the fuel inlet is within the range of [300, 1200]. With the increase of Re, the calculated temperature changes from a steady state to a periodic unstable oscillation state, and the height of the calculated flame increases continuously.

(2) The relationship between the flame flickering frequency St and Fr is fitted as $\mathrm{St} = 0.7\mathrm{Fr}^{-0.46}$.

(3) The nonlinear analysis indicates that the asymmetric phenomenon of the flame structure is a typical dynamic bifurcation, which evolves from a steady state to a flickering state with the increase of Re number.

(4) Three critical Reynolds numbers are identified to evaluate the state of the flickering flame: (i) when Re < 300, the flame keeps in the steady stable, (ii) when 300< Re < 1200, the flame starts to flickering and the temperature distribution of flame is asymmetric, (iii) when Re > 1200, flame appeared apparently flickering and the system stays in the chaotic state.

ACKNOWLEDGEMENTS

WL, MY, and XY acknowledge the support of the Chinese Natural Science Foundations under Grant No. 51736007.

REFERENCES

Araya, Y., Ito, H., and Kitahata, H., 2022, “Bifurcation Structure of the Flame Oscillation,” *Physical Review E,* **105**(4), 044208. https://dx.doi.org/10.1103/PhysRevE.105.044208.

Bennett, B. A. V., McEnally, C. S., Pfefferle, L. D., and Smooke, M. D., 2000, “Computational and Experimental Study of Axisymmetric Coflow Partially Premixed Methane/Air Flames,” *Combustion and Flame*, **123** (4), 522–546.

https://dx.doi.org/10.1016/S0010-2180(00)00158-9.

Bae, J., Jo, H., and Yoon, Y., 2022, “Instability Prediction of GO2/GCH4 Flames in a Single Recessed Coaxial Injector Using 1D Lumped Network Model,” *Journal of Mechanical Science and Technology*, **36**, 5755–5764. https://dx.doi.org/10.1007/s12206-022-1037-2.

Fujisawa, N., Yamada, J., and Yamagata, T., 2014, “Measurement of Three-Dimensional Temperature Field of Flickering Premixed Flame

Global Digital Central
ISSN: 2151-8629

with and without Coflow," *Flow, turbulence and combustion,* **93**(4), 723–739.
https://dx.doi.org/10.1007/s10494-014-9568-y.

Fujisawa, N., and Okuda, T., 2018, "Effects of Co-Flow and Equivalence Ratio on Flickering in Partially Premixed Flame," *International Journal of Heat and Mass Transfer,* **121,** 1089–1098.
https://dx.doi.org/10.1016/j.ijheatmasstransfer.2018.01.072.

Hariharan, A., and Wichman, I. S, 2014, "Premixed Flame Propagation and Morphology in a Constant Volume Combustion Chamber," *Combustion Science and Technology* **186** (8), 1025–1040.
https://dx.doi.org/10.1080/00102202.2014.897340.

Krikunova, A., Saveliev, A., and Cheshko, A., 2022, "Inverted Conical Methane/Air Flame Shape Transformation under Acoustic Excitation: Gravity Impact," *Physics of Fluids*, **34** (6), 061704.
https://dx.doi.org/10.1063/5.0050260.

Li, Y., Yang, M., and Zhang, Y, 2021, "Asymmetric Phenomenon of Flow and Mass Transfer in Symmetric Cylindrical and Semi-Cylindrical Shallow Chambers," *International Communications in Heat and Mass Transfer*, **123,** 105174.
https://dx.doi.org/10.1016/j.icheatmasstransfer.2021.105174.

Li, Y., Yang, M., and Zhang, Y., 2021, "Bifurcation Analysis of Coupling Thermosolutal Convection Induced by a Thermal and Solutal Source in a Horizontal Cavity," *International Communications in Heat and Mass Transfer*, **126,** 105455.
https://dx.doi.org/10.1016/j.icheatmasstransfer.2021.105455.

Li, Y., Yang, M., and Wang, Z. Y., 2019, "Study on heat and mass transfer with heat and mass and nonlinear characteristics source in cavity," *Frontiers in Heat and Mass Transfer,* **13**(11).
https://dx.doi.org/ 10.5098/hmt.13.11.

Manikantachari, K., Raghavan, V., and Srinivasan, K., 2011, "Natural Flickering of Methane Diffusion Flames," *International Journal of Mechanical and Mechatronics Engineering,* **5**(11), 2416–2421.
https://dx.doi.org/10.5281/zenodo.1061856.

Massa, L., and Freund, J. B., 2017, "Plasma-Combustion Coupling in a Dielectric-Barrier Discharge Actuated Fuel Jet," *Combustion and Flame,* **184**, 208–232.
https://dx.doi.org/10.1016/j.combustflame.2017.06.008.

Mohammadpour, K., Chitsazan, A., and Specht, E., 2022, "Consideration of influencing parameters on the flame length in parallel flow regenerative shaft kilns using porous media model," *Frontiers in Heat and Mass Transfer,* **19**(34).
http://dx.doi.org/10.5098/hmt.19.34.

Oyewola, O.M., Ismail, O.S., and Bosomo, J.O., 2021, "Numerical Simulations of the Effect of Turbulence in the Thermal-radiation Flow Field," *Frontiers in Heat and Mass Transfer,* **17**(8).
http://dx.doi.org/10.5098/hmt.17.8.

Sciamanna, M., and Shore, K. A., 2015, "Physics and Applications of Laser Diode Chaos," *Nature photonics*, **9**(3), 151–162.
https://dx.doi.org/10.1038/nphoton.2014.326.

Sayed-Kassem, A., Elorf, A., Gillon, P., Idir, M., Sarh, B., and Gilard, V., 2021, "Numerical Modelling to Study the Effect of DC Electric Field on a Laminar Ethylene Diffusion Flame," *International Communications in Heat and Mass Transfer*, **122**, 105167.
https://dx.doi.org/10.1016/j.icheatmasstransfer.2021.105167.

Sayed-Kassem, A., Gillon, P., Idir, M., and Gilard, V., 2022, "Flickering of a Diffusion Flame: An Innovative Way of Stabilization by a Mechanical Actuator," *International Communications in Heat and Mass Transfer*, **139**, 106475.
https://dx.doi.org/10.1016/j.icheatmasstransfer.2022.106475.

Singh, P., Velamati, R. K., and Chander, S., "Effect of Obliquity on Impingement Heating Characteristics of Co-Axial Swirling Flame Jet-An Experimental and Numerical Investigation," *International Communications in Heat and Mass Transfer*, **139**, 106474.
https://dx.doi.org/10.1016/j.icheatmasstransfer.2022.106474.

Wang, Q., Huang, H. W., Tang, H. J., Zhu, M., and Zhang, Y., 2013, "Nonlinear Response of Buoyant Diffusion Flame under Acoustic Excitation," *FUEL*, **103**, 364–372.
https://dx.doi.org/10.1016/j.fuel.2012.08.008.

Xu, C., Liu, W., Oppong, F., Wang, Q., Sun, Z.-Y., and Li, X., 2022, "Investigations on Cellularization Instability of 2-Ethylfuran," *Renewable Energy*, **191**, 447–458.
https://dx.doi.org/10.1016/j.renene.2022.04.068.

Yoshihara, N., Ito, A., and Torikai, H., 2013, "Flame Characteristics of Small-Scale Pool Fires under Low Gravity Environments," *Proceedings of the Combustion Institute*, **34** (2), 2599–2606.
https://dx.doi.org/10.1016/j.proci.2012.06.088.

Yamamoto, K., He, X., and Doolen, G. D., 2004, "Combustion Simulation Using the Lattice Boltzmann Method," *JSME International Journal Series B Fluids and Thermal Engineering*, **47** (2), 403–409.
https://dx.doi.org/10.1299/jsmeb.47.403.

Yang, L., 2018, "Fighting Chaos with Chaos in Lasers," *Science*, **361** (6408), 1201–1201.
https://dx.doi.org/10.1126/science.aau6628.

Ying, X., Huang, W., Liu, W., Liu, G., Li, J., and Yang, M., 2022, "Asymmetric Phenomenon of Flow and Heat Transfer in Charging Process of Thermal Energy Storage Based on an Entire Domain Model," *Applied Energy*, **316**, 119122.
https://dx.doi.org/10.1016/j.apenergy.2022.119122.

Zhang, H., Xia, X., and Gao, Y., 2021, "Instability Transition of a Jet Diffusion Flame in Quiescent Environment," *Proceedings of the Combustion Institute*, **38** (3), 4971–4978.
https://dx.doi.org/10.1016/j.proci.2020.07.086.

Zhu, F., Huang, X., and Wang, S., 2022, "Flame Spread over Polyethylene Film: Effects of Gravity and Fuel Inclination," *Microgravity Science and Technology*, **34** (3), 1–14.
https://dx.doi.org/10.1007/s12217-022-09945-4.